ELSEVIER

Polymer 43 (2002) 6943–6953

polymer

www.elsevier.com/locate/polymer

Poly(imide–amide)–poly(ethylene adipate) hybrid networks. I. Nanostructure and segmental dynamics

V.A. Bershtein[a,*], V.M. Egorov[a], L.M. Egorova[a], P.N. Yakushev[a], L. David[b], P. Sysel[c], V. Sindelar[c], P. Pissis[d]

[a]*Ioffe Physico-Technical Institute of the Russian Academy of Sciences, 194021 St Petersburg, Russian Federation*
[b]*GEMPPM, UMP-CNRS 5510, INSA Lyon, 69621 Villeurbanne Cedex, France*
[c]*Department of Polymers, Institute of Chemical Technology, 5 Technicka, 16628 Praha 6, Czech Republic*
[d]*Department of Physics, National Technical University of Athens, 15773 Athens, Greece*

Abstract

Segmental dynamics at 200–500 K and nanometer-scale structure were studied by SAXS, DSC and creep rate spectroscopy (CRS) techniques in two series of poly(ethylene adipate)-crosslinked poly(imide–amide)s with regularly varied composition and different lengths of PEA crosslinks (M_n = 1.300 and 2.700 g mol^{-1}). The crystallization ability was observed in networks with longer PEA crosslinks. Shorter PEA crosslinks induced non-crystalline, nanostructured PIA–PEA networks. Combined DSC/CRS analysis indicated the pronounced heterogeneity of segmental dynamics in the latter networks. The wide dispersions of motional activation energies within the glass transitions were found by DSC, and manifestation of a few constituent segmental motions was shown in the creep rate spectra. The observed effects could be explained in terms of (i) the different constraining influence of PIA rigid constituents on dynamics in PEA crosslinks, and (ii) the breakdown of motional cooperativity as a result of loosening of PEA chain packing in presence of the PIA rigid nanodomains.

Keywords: Poly(ethylene adipate)-crosslinked poly(imide–amide); Hybrid polymer networks; Constrained dynamics

1. Introduction

The industrial importance of membrane technologies has greatly increased in the last decades, in particular, for separation of volatile organic compounds from air. The membranes prepared from elastomers were successfully tested for these aims [1–3]. However, for the separation of heat solvent-containing air streams, the membranes with not only both high permeability and good selectivity but also with improved, acceptable thermal, mechanical and solvent resistance are needed.

Such high-performance materials such as polyimides (PIs) show high selectivity for separation of mixtures of air gases but too low permeability for both these gases and organic vapors [4]. These polymers are normally insoluble and intractable in their fully imidized form. The tractability and improved membrane properties of PIs could be attained by incorporation of flexible polymer chains into their structure. Thus, the membranes, based on linear poly(imide–dimethylsiloxane) block copolymers, showed a large increase in the permeabilities to organic vapors in comparison with PIs. However, the irreversible changes of the copolymer structure after penetration of the organic medium resulted in irreproducibility [4]. The membrane based on poly(ether–imide) materials were successfully employed in separation of organic vapors from air gases [5,6].

Of special interest may be the crosslinked PI-flexible chain hybrid materials with increased overall (thermal, mechanical and solvent) resistance.

In our previous publication [7], the promising results in this relation were obtained for poly(imide–amide)–poly(ethylene adipate) (PIA–PEA) hybrid networks, i.e. for the membranes synthesized from PIA crosslinked with PEA. As shown, very low permeabilities were observed for both PI and 50PIA–50PEA networks whereas the permeability coefficients of organic vapors in the membranes with 60 or 80% PEA were 2–3 orders of magnitude higher than those of gases (N_2, O_2, CO_2). This was associated with increased solubility of organic molecules in PIA–PEA membrane and their influence as the plasticizers enhancing segmental mobility and diffusion processes. An important property of

* Corresponding author. Tel.: +7-812-2479172; fax: +7-812-2478924.
E-mail address: vbersht@polmater.ioffe.ru (V.A. Bershtein).

0032-3861/02/$ - see front matter
PII: S0032-3861(02)00665-1

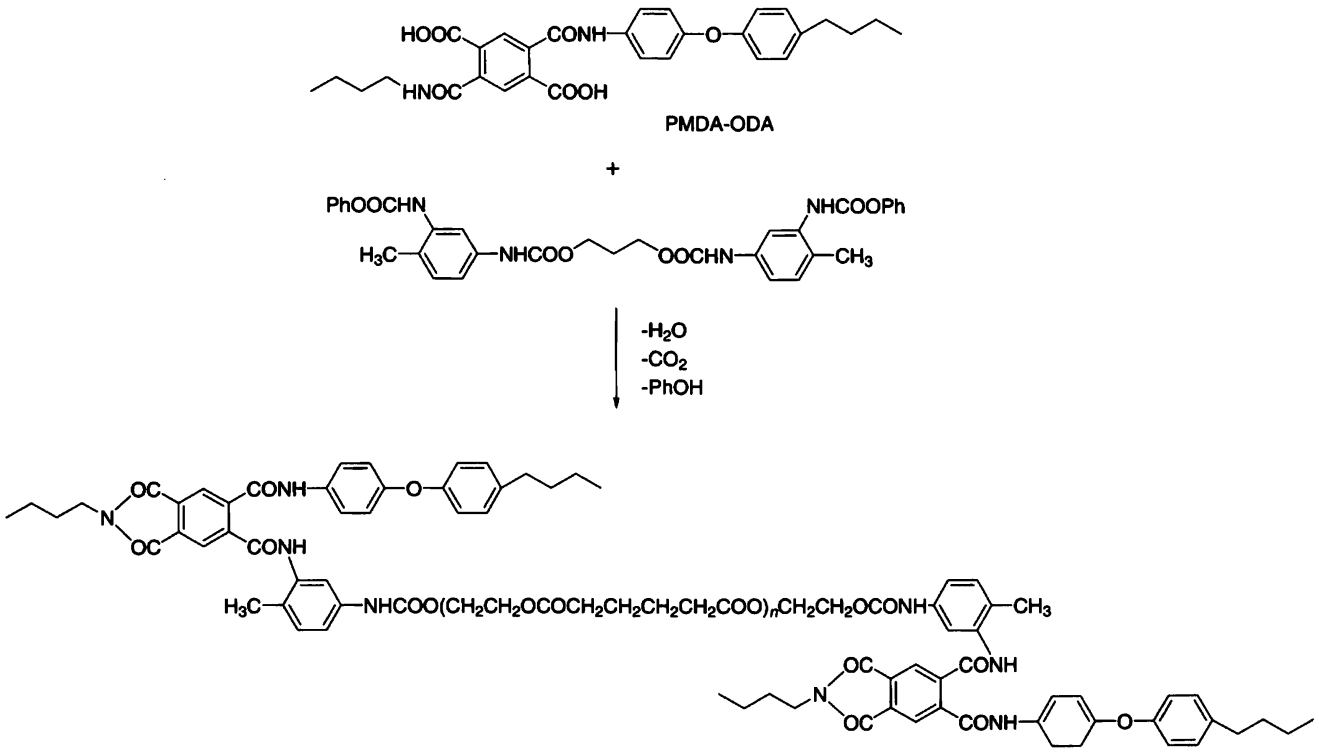

Scheme 1.

these network membranes was the resistance to penetrants (organic molecules).

Since segmental mobility really determines, to a large extent, the transport processes through membranes, the objective of present work was to clarify the peculiarities of dynamics and nanostructure in PIA–PEA hybrid networks depending on their composition, crosslink concentration and PEA molar mass, i.e. the length of flexible crosslinks. In addition, such networks are of interest for fundamental study of dynamics in chains covalently anchored from both ends to rigid constituents (PIA chains).

2. Experimental

2.1. Materials

PIA–PEA networks were synthesized in accordance with the procedures described [7–9]. The starting materials were (a) poly(amic acid) as the PI precursor, based on pyromellitic dianhydride and 4,4′-oxydianiline [PAA(PMDA–ODA)], and (b) toluene-2,4-diisocyanate terminated poly(ethylene adipate), where the remaining isocyanate groups were end-capped with phenol [Ph–TDI–PEA]; the latter permitted to prevent the premature reaction between both components, PAA(PMDA–ODA) and Ph–TDI–PEA, during their mixing. Ph–TDI–PEA with two different number average molar masses, $M_n = 1.300$ g mol^{-1} and 2.700 g mol^{-1}, were used in the experiments.

PAA(PMDA–ODA) with uncontrolled molecular weight was prepared by the reaction of equimolar amounts of a dianhydride and a diamine in the solvent, 1-methyl-2-pyrrolidone (NMP, Merck) (solid content 10 wt%) at room temperature for 24 h. Pyromellitic dianhydride (PMDA) was heated overnight to 160 °C in vacuum before use. 4,4′-Oxydianiline (ODA), TDI–PEA and phenol (all Aldrich) were used as received. NMP was distilled in vacuum over phosphorus pentoxide and stored in an inert atmosphere.

PAA solution in NMP and Ph–TDI–PEA were mixed at room temperature for 2 h in various weight ratios. The PAA/Ph–TDI–PEA mixtures (or pure components) in NMP were cast onto a glass plate. After evaporating the solvent, the films based on the mixtures were subjected to thermal treatment at 150, 200 and 250 °C for 1, 2 and 1 h, respectively. The films based on PAA(PMDA–ODA) only were treated at 150, 200, 300 and 330 °C for 1, 2, 1 and 0,5 h, respectively. The final transparent films with a thickness of ca. 40–50 μm were obtained.

During the thermal treatment, phenol was released and the deprotected isocyanate groups of TDI–PEA reacted with the carboxylic groups of PAA(PDMA–ODA) with formation of amide groups. Consequently, two reactions, both PAA imidization and crosslinking (hybridization of both components), proceeded in parallel on heating (Scheme 1).

As a result, the networks formed were quite complicated in their structures, and contained basically imide groups in backbone and ester groups in crosslinks and also the amide and urethane groups in backbone and crosslinks,

respectively. The more crosslinking agent content (Ph–TDI–PEA) was introduced in a composition, the more quantity of crosslinks between PI chains and the more content of amide groups in the latter were formed; this was confirmed by IR spectroscopy [7]. It should be mentioned that the term 'poly(imide–urethane) networks' was earlier applied to similar materials [8,9]. Nevertheless, we prefer to consider these networks as poly(imide–amide)–poly(ethylene adipate) (PIA–PEA) hybrids, indeed, or PIA crosslinked with PEA [7].

On the whole, besides pure linear PI and PEA network, two series of hybrid networks were studied, viz. (1) with 'short' PEA crosslinks ($M_n = 1.300$ g mol^{-1}) and PIA/PEA weight ratios of 10/90, 20/80, 30/70, 40/60, and 50/50, and (2) with 'long' PEA crosslinks ($M_n = 2.700$ g mol^{-1}) and PIA/PEA weight ratios of 20/80, 50/50, 60/40, and 80/20.

2.2. SAXS measurements

The small angle X-ray scattering (SAXS) technique was applied for estimation of the nanometer-scale structure of PIA–PEA networks with short PEA crosslinks and 10, 20, 30 or 50 wt% PEA, and for pure components, linear PI and PEA network. The experiments were carried out using a copper rotating anode (Rigaku), in point collimation conditions, using crossed Ni-coated total reflection Franck mirrors, and a sealed methane/xenon linear detector (INEL). The raw spectra were corrected for background scattering. The experiments were performed twice for each sample.

2.3. Differential scanning calorimetry

DSC curves were measured over the temperature range from 220 to 500 K using the Perkin–Elmer DSC-2 apparatus calibrated with water (273.1 K), cyclohexane (279.6 K), and indium (429.8 K). The heat capacity scale was calibrated using sapphire. The experiments were carried out in a nitrogen atmosphere. The heating rates of $V = 1.25$, 2.5, 5, 10, 20 and 40 K min^{-1} were used; the standard rate was 10 K min^{-1}. Reproducible DSC curves were obtained at the second and following scans, after heating to 500 K ($V = 10$ K min^{-1}) with subsequent cooling down to 220 K at $V = 320$ K min^{-1}.

A few characteristic temperatures on the DSC curves at $T < 400$ K were estimated, which are related to the transitions in the PEA component. These included, in particular, the temperatures in heat capacity steps (glass transitions), T_g at the half-height of a step, and the onset, T_g', and completion, T_g'', temperatures of the transition ranges. On this basis, the effective activation energy Q of segmental motion as a function of temperature over the temperature range, covering one or more glass transitions, observed on the DSC curve of the hybrid network, were determined for stabilized samples by displacement of the above temperatures with a heating rate, using the formula:

$$Q = -R \, \mathrm{dln}\, V/\mathrm{d}(1/T) \quad (1)$$

Validity of this formula has been shown by the theoretical analysis and experiments [10], and then by the numerous DSC estimates of Q values for glass transition and other relaxations, by comparing with the Q estimates made by the other techniques, e.g. by DMA [11]. In this case, each Q value is determined for narrow temperature range, typically 5–10°, by changing V not more than by an order of magnitude. Under these conditions, linear ln V versus $1/T$ plots are normally observed.

The crystallization peak temperatures, T_{cr}, melting temperatures, T_m, and crystallinities of the PEA component, χ, were also determined in the case of the crystallizable hybrid networks with the longer PEA crosslinks of $M_n = 2.700$ g mol^{-1}. The accuracy of characteristic temperatures, T_g, T_{cr}, T_m, ΔC_p steps, Q and χ determination was equal to ± 1 K, $\pm 5\%$, $\pm 10\%$, and $\pm(3–10)\%$, respectively. It was difficult to analyze glass transition in PIA component by DSC due to the masking effects of PEA destruction at $T > 500$ K.

2.4. Creep rate spectroscopy

Laser-interferometric creep rate spectroscopy (CRS) was used for the discrete analysis of molecular mobility in the samples under study over the temperature range from ca. 180 to 500 K. The scheme of the used CRS setup, operating under tension, and the experimental technique have been described in detail elsewhere [12–16].

The CRS method consists in precise measuring of low creep rates at constant small stress, much less than the yield stress, as a function of temperature (creep rate spectrum). A laser interferometer based on the Doppler effect is used for this aim. The time evolution of deformation is registered as a sequence of low-frequency beats in an interferogram whose beat frequency ν yields a creep rate

$$\dot{\varepsilon} = \lambda\nu/2I \quad (2)$$

where $\lambda = 630$ nm is the laser wavelength, and I is the length of the working part of the sample. The film samples with ca. 0.1×4 mm^2 crosssection and $I = 20$ mm were used. The tensile stress of 0.5 or 3 MPa were chosen as capable of inducing sufficient creep rates to be measured while maintaining a high spectral resolution.

Under a low stress, creep is associated with local shear strain, and its rate decreases as the creep process proceeds. Therefore, besides the stress, the second experimental parameter, time from the moment of loading to the onset of measurement was kept constant ($t = 10$ or 30 s) at the time of measuring a creep rate spectrum. The correlative frequency of the CRS experiments was $\nu_{corr} = (2\pi t)^{-1} = 10^{-3}–10^{-2}$ Hz, i.e. time conditions were close to those in the DSC experiments.

Normally, a sample was cooled down to the lowest

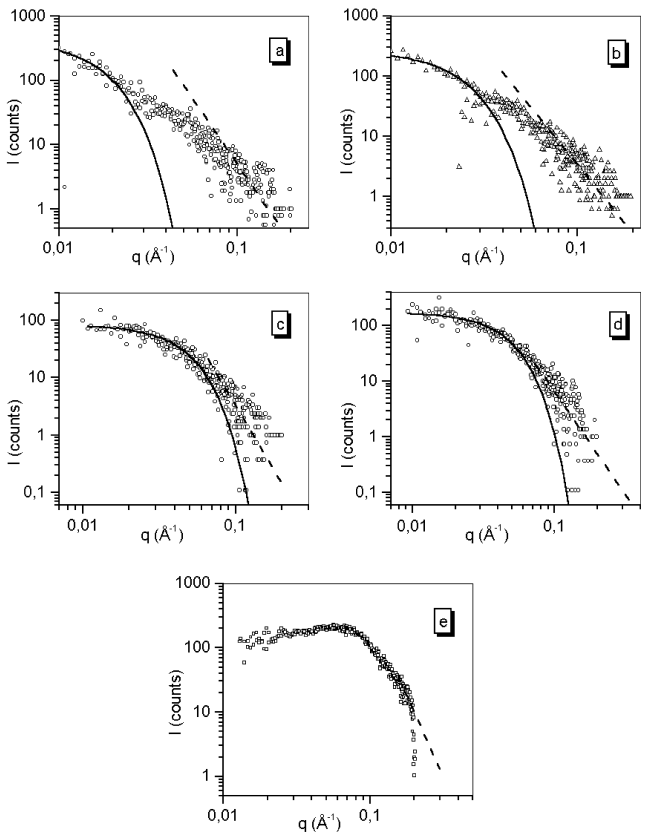

Fig. 1. SAXS patterns obtained for the non-crystalline hybrid networks with short PEA cross-links(M_n = 1300 g mol^{-1}) and PIA/PEA weight ratios: (a) 10/90; (b) 20/80; (c and d, repeated measurements) 30/70, and (e) 50/50. Solid lines correspond to Guinier's law, and dashed lines to Porod's asymptotes.

temperature range under study, and the small stress was applied for 1 min to get the interferogram. Then, the sample was unloaded, heated at the rate of 1 K min^{-1} to a temperature of 5 K higher, and was loaded again at the same stress. Again, the interferogram was registered; the sample was unloaded and so on. The sample was set in the special clamps providing immobile, fixed position; this was controlled by total recovery of deformation after unloading, during a subsequent 5 min heating. Typically, the multiple peaks of increased creep rates appeared on the creep rate versus T curves, measured in the way described, as a response to unfreezing of different kinds of molecular motions.

Table 1
Nanostructure of the PIA–PEA networks with the shorter crosslinks

PIA/PEA weight ratio	Intraparticular size R_g (nm)	Interparticular size d (nm)
10/90	3.5–10	>30
20/80	3.5–7.5	>30
30/70	3.5	>30
50/50	2.0	7.5

The CRS superiority in resolution and sensitivity to widespread relaxation spectrometry techniques has earlier been shown in the above publications. CRS technique allowed us to measure creep rates on the basis of deformation increment of ca. 0.01–1%. The instrumental accuracy of separate creep rate measuring was not worse than 1%. At the same time, scattering at repeated measurements may be higher, by one order of magnitude, due to differences in sample state, loading conditions, etc. Nevertheless, satisfactory reproducibility of the CR spectra, including manifestation of the same set of constituent creep rate peaks, and their relative intensities, has been observed (see Fig. 7 in Ref. [17]).

3. Results and discussion

3.1. Nanostructure

The SAXS measurements were carried out for the hybrid networks with short PEA crosslinks.

The pure PI and PEA systems exhibited very low scattering and could be considered as homogeneous in the range of 1–40 nm. SAXS scattering patterns, obtained for the hybrid networks with 50 (e), 70 (c and d), 80 (b) and 90 wt% PEA (a), are given in Fig. 1. Numerical evaluations are given in Table 1.

The SAXS spectra of the 30PIA–70PEA network (Fig. 1(c) and (d)) display a well defined Guinier's behavior at low angles, synonym of scattering by nanoscopic domains with roughly spherical geometry and randomly distributed in a matrix. Consequently, the spectra could be analyzed through Guinier's law

$$I(q) = I_0 \exp(-q^2 R_g^2/3) \quad (3)$$

where qRg is not $\gg 1$, R_g is the intraparticular size (gyration radius of the particles), q is the scattering vector ($q = 4\pi \sin Q/\lambda$), and $2Q$ is the scattering angle. At larger angles, for $q > 0.07\text{A}^{-1}$, the SAXS pattern exhibited a Porod's law behavior ($I = C/q^4$).

Such pattern features are characteristic of particles (obviously, PIA-rich domains) with narrow size distribution and with sharp interfaces, embedded in a PEA-rich matrix (R_g = 3.5 nm, d > 30 nm, see Table 1).

The 50PIA–50PEA network exhibits a well defined maximum indicative of interference effects between the particles (Fig. 1(e)). In this case, the scattering pattern thus corresponds to a relatively ordered nanostructure with a periodicity close to 7.5 nm and a gyration radius of particles $R_g \approx$ 2.0 nm. The Porod's behavior could also be observed. For a more reliable determination of the size of the particles and accounting for the masking interference effects at low q values, the Beacage model [18] (structure factor $S(g)$ of hard spheres, a Porod term and a Guinier term for the

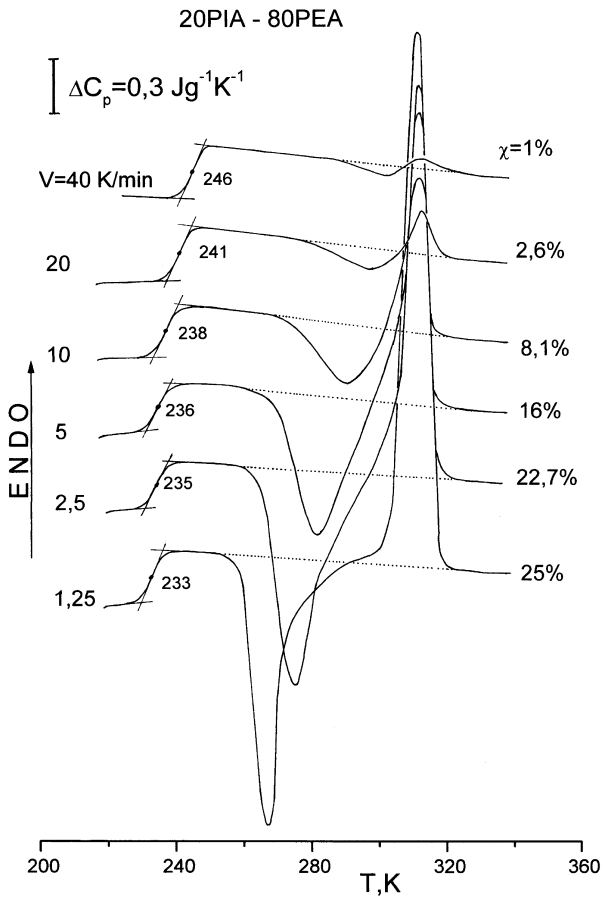

Fig. 2. DSC curves of the 20PIA–80PEA hybrid network with the longer PEA crosslinks ($M_n = 2.700$ g mol^{-1}) obtained at indicated heating rates. Second scans after heating to 500 K with subsequent cooling down to 220 K with $V = 320$ K min^{-1}. The crystallinities of PEA component are indicated.

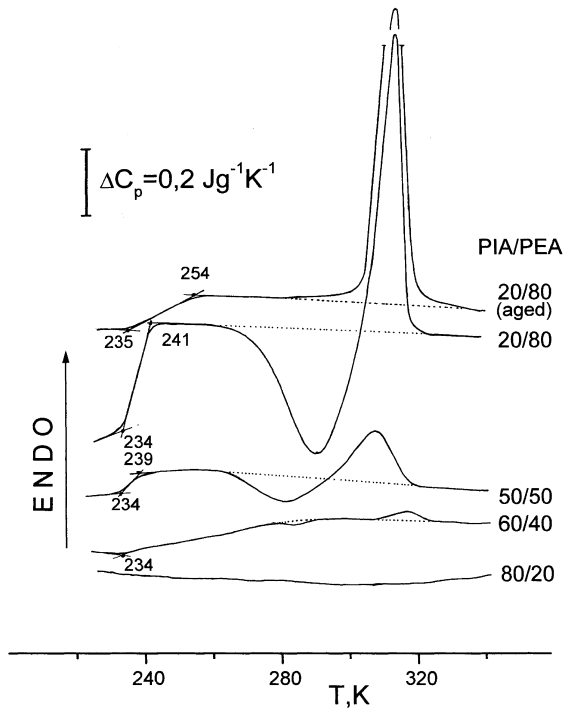

Fig. 3. DSC curves of the networks with the longer PEA crosslinks ($M_n = 2.700$ g mol^{-1}) and PIA/PEA weight ratios of 20/80, 50/50, 60/40, and 80/20. Heating rate $V = 10$ K min^{-1}. Second scans after heating to 500 K with subsequent cooling down to 220 K with $V = 320$ K min^{-1}. The aged 20PIA–80PEA network was obtained after 9-day staying of the treated sample at 293 K.

isolated particle scattering) was applied to extract numerical data.

Nevertheless, as the volume fractions of both rigid and flexible constituents are close, non-particulate phase arrangements are possible in this case, such as co-continuous structures.

The periodicity distance (about 7.5 nm) can still be considered to be a valid parameter to evidence the nanostructure of these systems. Assuming a morphology constituted by pure PEA and PIA phases, the characteristic lengths of the system can be calculated with the Porod's asymptote according to [19]:

$$l_{PEA} = 4Q/[\pi C(1 - \Phi_{PEA})]$$

$$l_{PIA} = 4Q/[\pi C(1 - \Phi_{PIA})]$$

with

$$Q = I(q)q^2\,dq \qquad \text{and} \qquad \Phi_{PIA} + \Phi_{PEA} = 1$$

where Q is the invariant and C is the Porod's constant, l_{PEA} and l_{PIA} are the mean cord lengths, Φ_{PEA} and Φ_{PIA} are the volume fractions of PIA and PEA, respectively, deduced from the mass fractions (0.5) and the densities of PEA ($\rho_{PEA} \sim 1.2$ g/cm^3) and PIA ($\rho_{PIA} \sim 1.4$ g/cm^3). The values found for l_{PEA} and l_{PIA} turned out to be close again to 3 nm, comparable to the gyration radius R_g obtained assuming a particulate morphology.

Finally, the 10PIA–90PEA and 20PIA–80PEA systems turned out to be more difficult to analyze. The simple Guinier behavior was not observed in these cases. This could be due to a wide range of characteristic intraparticular sizes. The solid lines appearing in the low q range of these spectra (Fig. 1(a) and (b)) can be considered as Guinier's law the largest size that can be deduced from the experimental data. At the same time, the Porod's behavior was still present in about the same q range, thus revealing that the size of the smallest particles should be similar to that in the 30PIA–70PEA system.

3.2. DSC data

Figs. 2 and 3 show the DSC curves obtained on heating the PIA–PEA networks with the longer PEA crosslinks quickly cooled in a calorimeter from 500 to 220 K with the rate of 320 K min^{-1}. The temperature range investigated (220–370 K) covers glass transition region and phase transitions (i.e. crystallization and melting) in PEA, as the equilibrium melting point of a perfect PEA crystal is equal to 338 K [20]. There were no distinct thermal transitions on these DSC curves at higher temperatures; at $T > 500$ K, the

exotherms were associated with the onset of degradation process in PEA component.

Fig. 2 shows the narrow glass transition range, $\Delta T_g = T_g'' - T_g' = 7\ K$, and $T_g = 238$ K, at $V = 10$ K min^{-1}, for the 20PIA–80PEA network with the longer crosslinks. Displacement of the transition temperatures, T_g', T_g and T_g'', with heating rate and the calculations by using the formula Eq. (1) indicated the invariable effective activation energy $Q \approx 170$ kJ mol^{-1} within this narrow glass transition range (see below Fig. 6, dependence 1). Such Q behavior and high value are typical of cooperative segmental dynamics in the absence of dynamic heterogeneity within glass transition [11]. It should be mentioned that PEA crosslink in this case ($M_n = 2.700$ g mol^{-1}) involves about 10 statistical Kuhn segments, each with the length of ca. 2 nm. The characteristic size involved in the cooperative motion in the glass transition in PEA can thus be thought to be much lower than 20 nm.

Figs. 2 and 3 also show that the longer PEA crosslinks in the networks under study are capable of a partial crystallization, and the crystallinities being attained depend on both heating rate (Fig. 2) and network composition (Fig. 3). Unlike typical crystallization processes in linear polymers, the crystallinity of PEA component in the 20PIA–80PEA network drastically changed with heating rate, from $\chi = 25\%$ in the case of slow heating of the quickly cooled sample down to $\chi = 1$–2% at the heating rates of 20–40 K min^{-1}. Moreover, a large displacement of the maximum of the exothermic crystallization peak with a heating rate (by 36 K) can be observed. Large reduction of crystallization ability is obviously the result of the presence of the rigid PIA phase limiting long-scale motions of the PEA chains, which are necessary for nucleation and diffusion processes. The small difference, of ca. 10 K, between crystallization and melting peaks is observed at $V = 40$ K min^{-1} (Fig. 2).

The drastic changes in thermal behavior of the longer PEA crosslinks with increasing PIA content in the hybrid networks from 20% to 50, 60 and 80% are seen from Fig. 3. Introducing 50% PIA into the network resulted in a large reduction of both heat capacity step at T_g and the crystallization and melting peak areas. Only very slight traces of the indicated phase transitions may be discerned on the DSC curve of the 60PIA–40PEA network. Simultaneously, a broadening of the glass transition range to higher temperatures is observed in this case; it extended from 234 to about 280 K. Somewhat broadened ΔT_g range is also observed for the aged, partly crystallized sample with the lesser PIA content (Fig. 3). This ΔT_g broadening effect is obviously associated with the different constraining influence of rigid phase on PEA dynamics, and 'unfreezing' of PEA segmental motion at different temperatures (see below).

At last, in the 80PIA–20PEA network the thermal transitions, i.e. cooperative glass transition, or crystallization and melting, could not be discerned at all on the DSC curve (Fig. 3). Thus, the hybrid networks with the longer PEA crosslinks and 60 – 80 wt% PIA are practically amorphous products. One may assume that increased distances between the sparse PEA crosslinks in the PIA-rich hybrid networks prevented formation of PEA nanodomains, i.e. manifestation of cooperative dynamics or ordering process. Thus, the presence or absence of glass transition is controlled not only by the individual length of the PEA crosslinks; it is also governed by the possibility of the PEA segments of different crosslinks to be grouped in order to form a phase of sufficient volume to exhibit the glass transition.

Fig. 4 shows the DSC curves obtained at 230–390 K for pure PEA network and a series of PIA–PEA hybrid networks containing the shorter PEA crosslinks ($M_n = 1.300$ g mol^{-1}). The glass transition characteristics of these networks are given in Table 2.

These results indicate quite different dynamic behavior of the shorter PEA crosslinks as compared to that of the longer ones. Firstly, the short PEA crosslinks, where each consisted of about five Kuhn segments only (representing a size of extended PEA chain of ca. 10 nm), were not able to form the ordered nanodomains; non-crystalline, nanostructured PIA–PEA networks were obtained. Secondly, T_g for the main PEA transition was higher than in the above networks with the longer crosslinks. Thirdly, a few heat capacity steps, i.e. 'plurality of glass transitions' in the PEA component of the networks with 10–40% PIA were observed at ~260–280, 300–320 and 330–340 K. Only one $T_g = 329$ K was found for the 50PIA–50PEA network (Fig. 4). At last, the summary ΔC_p value decreased with PIA content larger than it might be expected from the change in composition. Thus, five-fold ΔC_p reduction was observed on the DSC curve of the 50/50 hybrid network compared with ΔC_p for pure PEA network (Fig. 4, curves 1 and 6).

The DSC measurements, performed at different heating rates, allowed us to reveal the pronounced heterogeneity in

Table 2
Glass transition characteristics as estimated by DSC for short PEA crosslinks ($M_n = 1.300$ g mol^{-1}) in the PIA–PEA networks

PIA/PEA weight ratio	T_g (K)	ΔT_g (K)	ΔC_p (J g^{-1} K^{-1})
0/100	263	16	0.338
10/90	263	14	0.216
	274	11	0.043
20/80	268	23	0.169
	339	11	0.012
30/70	269	27	0.102
	304	9	0.030
	333	8	0.030
40/60	258	17	0.091
	318	5	0.017
	340	12	0.028
50/50	329	18	0.073

T_g, ΔT_g and ΔC_p values were measured at the heating rate of 10 K min^{-1}.

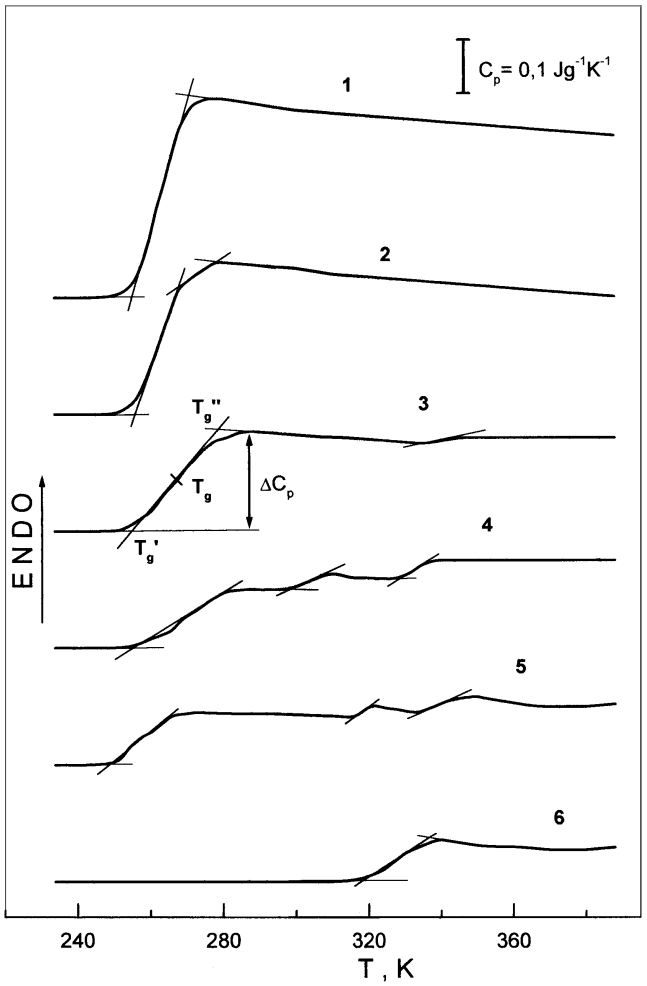

Fig. 4. DSC curves of the non-crystalline networks with the shorter PEA crosslinks ($M_n = 1.300$ g mol^{-1}) and PIA/PEA weight ratios: (1) 0/100; (2) 10/90; (3) 20/80; (4) 30/70; (5) 40/60, and (6) 50/50. Heating rate $V = 10$ K min^{-1}. Second scans after heating to 500 K with subsequent cooling down to 220 K with $V = 320$ K min^{-1}.

the glass transition dynamics for the short PEA crosslinks. As an example, Fig. 5 shows typical ln V versus T^{-1} plots, where T_g, T_g', and T_g'', displacements with a heating rate were determined for the 30PIA–70PEA network. The different slopes of the ln V (T^{-1}) dependencies imply the wide activation energy Q dispersion. By using such data and Eq. (1), the Q versus T dependencies were

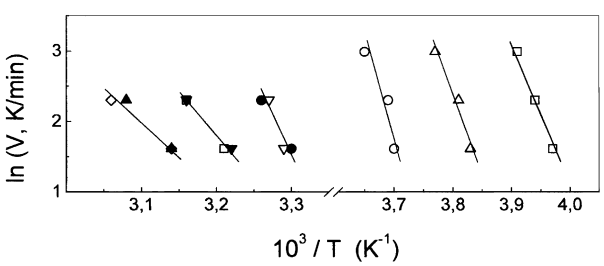

Fig. 5. Transition temperature versus logarithm heating rate plots obtained for a few characteristic PEA glass transition temperatures in the 30PIA–70PEA network (see curve 4 in Fig. 4).

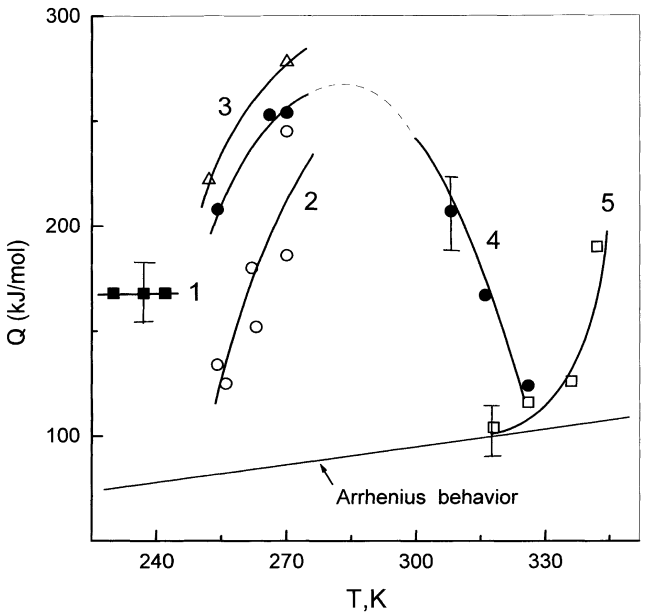

Fig. 6. Temperature dependence of the activation energy of segmental motion Q within the PEA glass transition ranges in the 20PIA–80PEA network with the (1) longer PEA crosslinks, (2) in pure PEA, (3) 10PIA–90PEA, (4) 30PIA–70PEA, and (5) 50PIA–50PEA networks with the shorter PEA sequences. Straight line corresponds to Q versus T dependence in the Arrhenius relation for any non-cooperative relaxation processes at the frequency of 10^{-2} Hz. Curve 2 indicates the results obtained at two repeated estimates.

estimated for segmental motion in the glass transitions of some PIA–PEA and pure PEA networks with the shorter ($M_n = 1.300$ g mol^{-1}) PEA sequences (Fig. 6, curves 2–5). The inclined straight line in this figure corresponds to a Q versus T plot for any non-cooperative relaxations obeying the Arrhenius relation for the frequency of motional events $f \approx 10^{13} \exp(-Q/RT)$, at the frequency $f \approx 10^{-2}$ Hz.

Curves 2–5 in Fig. 6 are of interest because they demonstrate the degree of Q deviation from Arrhenius behavior and indicate wide Q versus T dispersions, i.e. a large heterogeneity of PEA segmental dynamics within the glass transitions of the hybrid networks with the shorter crosslinks. One can see that curves 2–5 show virtually four different kinds of anomalous dynamic behavior, with three-fold Q variation, from about 100 to 280 kJ mol^{-1}.

It is noteworthy to be mentioned that unfreezing of segmental motion in glass transition of flexible-chain polymers is associated with intermolecular cooperative motions of Kuhn segments, where typically, parameter of cooperativity at low frequencies $Z \approx 4 \pm 1$; nevertheless, under certain conditions, in particular, in complex polymer systems (some block and graft copolymers, or plasticized polymers and so on) lower-cooperative or even non-cooperative segmental motion may be realized at T_g [11].

Therefore, the above Q dispersions (Fig. 6) may be

treated, as earlier for the other complex polymer systems [11,14,15,17,21–25], in terms of two opposite influences:

1. decreasing or total collapsing of intermolecular motional cooperativity around T_g due to loosening of chain packing, and
2. constraining influence of a rigid structural constituent on dynamics of 'soft' (PEA) component due to covalent anchoring of its chain ends to a rigid constituent.

If the first factor lead, in particular, to decreasing of the effective activation energy of segmental motion, the second one may lead to increasing T_g, ΔT_g range, Q values, and to possible manifestation of 'plurality of the glass transitions' as a consequence of different, by their magnitudes, constraining effects. It is clear that a segment directly attached to a rigid constraint (PIA), may be totally immobilized.

The $Q(T)$ curves 2–5 presented are in a total accordance with such approach and the simple common scheme, offered earlier [17,23,24] for explanation of the glass transition anomalies found in complex polymer systems of various types [11,14,15,17,21–25].

First of all, curves 2–5 are displaced to higher temperatures compared to curve 1, that indicates constraining effect in the case of the shorter PEA sequences. Comparison of curves 1 and 2 with each other shows arising of heterogeneity in glass transition dynamics in PEA network with the shorter interjunctional chains. In this case, Q ranges from ca. 120 to 250 kJ mol^{-1}, i.e. decreased, 'normal cooperative', and increased Q barriers to motion of different crosslink segments are simultaneously observed within the glass transition.

Introducing 10% PIA into PEA network resulted in the higher Q values (curve 3). Especially complicated, 'peaked' $Q(T)$ dependence was obtained for the 30PIA–70PEA network (curve 4) which manifested a few glass transitions. From a set of the Q values obtained, constrained cooperative, partly cooperative and practically non-cooperative segmental motions were involved into glass transition dynamics herein. The latter is also valid regarding a single glass transition in the 50PIA–50PEA hybrid network (curve 5).

As a matter of fact, participation of non-cooperative, Arrhenius segmental motions in glass transition dynamics is characteristic of the networks with the increased PIA content, i.e. with the increased distances between PEA crosslinks (see the minimal Q values in curves 4 and 5). Thus, Fig. 6 demonstrates, really, anomalous PEA glass transition dynamics with manifestation of both constrained dynamics and cooperativity breakdown effects.

3.3. Creep rate spectra

CRS analysis of segmental dynamics was carried out in a series of the samples including linear PI, pure PEA network and the PIA–PEA hybrid networks with the shorter crosslinks ($M_n = 1.300$ g mol^{-1}). The CR spectra obtained allowed us not only to confirm the pronounced heterogeneity of segmental dynamics in the region of glass transition but also to demonstrate, in a discrete manner, a few types of segmental motions constituting relaxation dynamics in this temperature range.

Figs. 7–10 show the CR spectra obtained under tension and indicated experimental conditions for pure components and four hybrid networks with 10, 20, 30 and 50 wt% PIA, mostly over the temperature range from 170 to about 400 K, and at 290–500 K for PI and the 50PIA–50PEA network.

Figs. 7 and 8 also include the insertions with the extended ordinate scale to represent the spectra more distinctly (Fig. 8) or to demonstrate the absence of CR peaks at $T < 250$ K for pure PEA network (Fig. 7). Besides, Fig. 8 shows rather similar CR spectra obtained at different creep times t, 10 or 30 s. Figs. 9 and 10 compare the CR spectra of the samples with 10, 20, 30 and 50% PIA, and pure PI.

The main result here is the existence of a single glass transition CR peak with maximum at ca. 280 K, obtained for pure PEA network that transforms into the complicated CR spectra of the hybrid networks, with the contours having a few partly overlapping constituents. The latter may manifest themselves as real peaks with distinct maximums, or such contour's peculiarities as a step or a 'shoulder' upon the edge of the larger neighboring peak. Up to 4–5 CR peaks (spectral components) may be observed in an each of the spectra of Figs. 8 and 9 at both higher and lower temperatures regarding the starting glass transition peak. At the same time, a large creep rate decreasing, by an order of magnitude, is observed on the whole at 200–400 K for the hybrid networks compared to pure PEA network.

For hybrid networks, besides the 'usual' glass transition peak remainder, one can see the spectral components at temperatures below 280 K, e.g. at about 220 and 250 K, which must be attributed to non- and low-cooperative PEA segmental relaxations, respectively. On the other hand, the components of the spectra at temperatures about 300–320, 350–360 and 380–390 K are observed and correspond, obviously, to increasingly constrained PEA segmental relaxations. The constraining effect may increase with reduction in a distance between a moving segment and rigid PIA chains. Very steep increasing of creep rates at 400–440 K is apparently associated with the onset of unfreezing of segmental mobility in PIA chains. Consequently, the CR spectra, obtained for the PIA–PEA hybrid networks, respond, really, in a discrete manner to unfreezing of a few kinds of segmental motions differing by intermolecular cooperativity or/and constraining degrees.

CR spectral shape depended on network composition. Fig. 9 shows that introducing 10% PIA into the network resulted in manifestation, besides decreased T_g peak at ~280 K, of constrained relaxations at higher temperatures only (curve 1). At the same time, introducing 20% PIA 'disturbed' supermolecular structure (molecular packing) of

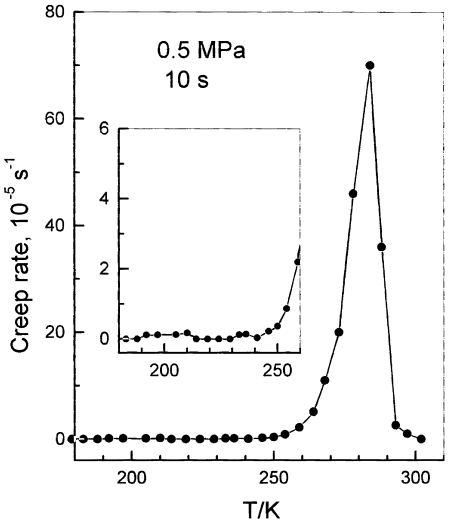

Fig. 7. Creep rate spectrum (glass transition peak) of pure PEA network (initial $M_n = 1.300$ g mol^{-1}) obtained at the indicated tensile stress and time. Insert shows a low-temperature part of the spectrum within an extended ordinate scale.

PEA to larger extent, and the CR spectral components at ~250 and 220 K, characterizing the reduced motional cooperativity, also arose (curve 2).

It should be mentioned that at high PEA content in these networks, e.g. 80%, a part of the PEA crosslinker remains unreacted in the hybrid network [7]. Some reduction of the CR peaks occurred after introducing of 30% PIA into the network (curve 3).

Strong suppression of segmental dynamics in PEA component at room and moderate temperatures was found in the case of the 50PIA–50PEA network. There was no distinct CR peaks at all in the spectra of this network and of pure PI at experimentation under the same 'standard' tensile

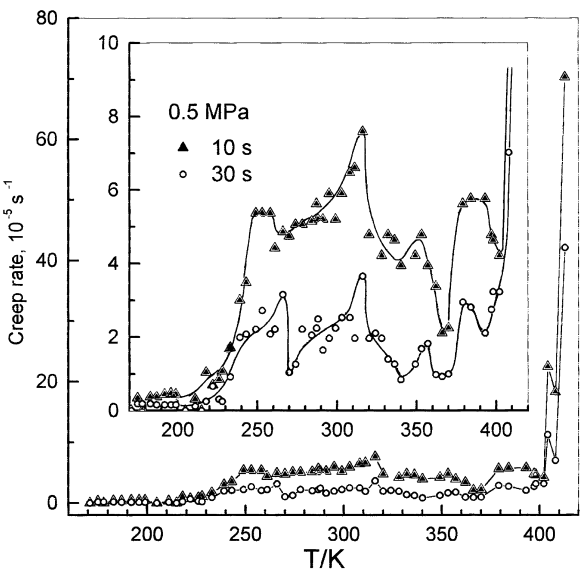

Fig. 8. Creep rate spectra of the 20PIA–80PEA network obtained under the indicated experimental conditions. Insert is given for an extension of the ordinate scale.

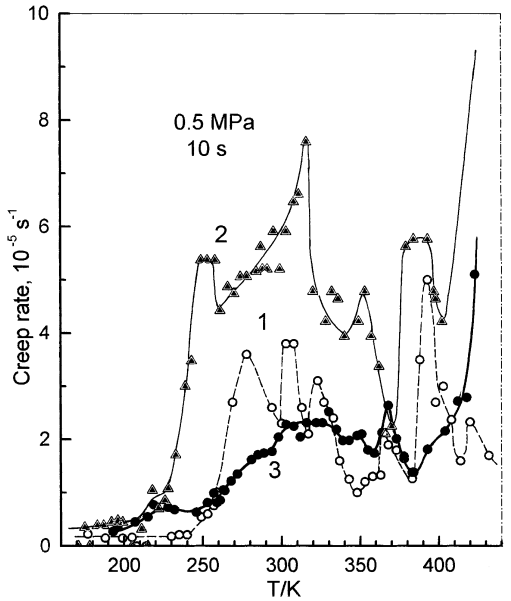

Fig. 9. Creep rate spectra of the (1)10PIA–90PEA, (2) 20PIA–80PEA, and (3) 30PIA–70PEA networks with the shorter crosslinks, obtained under the indicated experimental conditions.

stress of 0.5 MPa. Therefore, the stress of 3 MPa was used for these two samples. As one can see from Fig. 10, only traces of the CR peaks at ~340–380 K may be discerned in the spectrum of the 50/50 network. It should be noted that this network is characterized by the particularly fine nanometer-scale structure (Table 1), where the nanodomain and interdomain sizes are equal to 1–3 Kuhn segments only in PEA. As indicated above, the steep rise of creep rates starting from 440 K is associated with rising mobility in the PIA chains. Finally, for pure PI, the low creep rates were observed up to 520 K (Fig. 10).

It is noteworthy that the particularly prominent CR peaks are absent in the hybrid network spectra. The peaks observed are comparable by their heights and indicate the approximately close partial contributions of low-cooperative, cooperative as well as slightly or moderately, or strongly constrained motions to PEA segmental dynamics. This may be understood in terms of different PEA segment

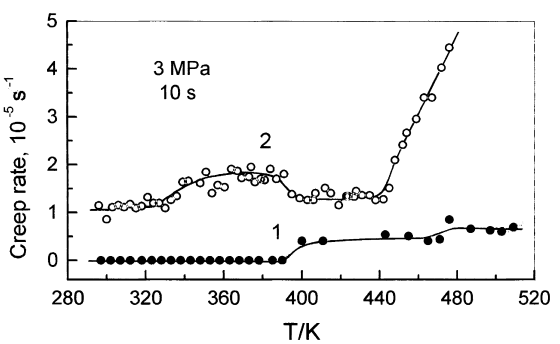

Fig. 10. Creep rate spectra of the (1) pure linear PI and (2) 50PIA–50PEA network with the shorter crosslinks, obtained under the indicated experimental conditions.

positions, within 5-segmental crosslink, regarding PIA constraints.

Thus, the CR spectra give more detailed dynamic picture than DSC data. It should be noted that there is no, on the whole, strict coincidence between CR spectral peaks position and the values of T_gs obtained by DSC (Figs. 4, 7–10). One can see rather good correlation for pure PEA network. For 50PIA–50PEA network, DSC glass transition is observed at 320–340 K but CR anomaly is observed at 340–380 K. Comparing Figs. 4 and 8 shows $T_g s$ at about 250–280, 300 and 330 K, whereas the largest CR spectral components at about 250–260, 320, 350 and 380 K are observed.

4. Conclusion

Segmental dynamics and nanostructure in two series of the PIA–PEA hybrid networks with regularly varied composition and different lengths of PEA crosslinks were studied in combined DSC/CRS/SAXS experiments over the temperature region of 200–400 K covering the main relaxation and phase transitions in the PEA crosslinker. Besides the fundamental interest in studying of hybrid polymer networks, this research was aimed at finding the connection between the properties of these networks, as new high-performance membranes for separation of organic vapors from air gases [7], and their dynamics and structural state.

The combined approach allowed us to reveal quite different nanostructural state and dynamic/thermal behavior of flexible PEA crosslinks depending on the hybrid composition and crosslink length, that directly affected the membrane properties of the films.

As found, special crystallization ability was observed for the longer PEA crosslinks only, whereas the hybrids with the shorter crosslinks (about five Kuhn segments in length) represented amorphous, nanostructured networks; the main attention was paid to the latter materials just studied in membranes [7].

All the data obtained for these PIA–PEA networks turned out to be in good accordance with their membrane properties, the experimental data [7] on their permeability for organic vapors.

Really, for the 50PIA–50PEA hybrids, a relatively 'ordered' nanostructure with a periodicity of a few nanometers was found that resulted in somewhat suppressed glass transition and increased T_g. Creep rate spectra also indicated suppressed PEA segmental mobility up to ~440 K. It was in accordance with a permeability of this network for organic vapors. Thus, the membranes, based on the 50PIA–50PEA and 80PIA–20PEA networks with suppressed mobility, showed behavior similar to that for pure PI membranes. Their permeability was so low that it was not possible to determine the corresponding coefficients [7].

Unlike that, the hybrid networks with lower PIA content, 10 or 20 wt%, have more random nanostructure. Much more intense segmental motion with a number of dynamic peculiarities was found by both DSC and CRS techniques in these cases. Thus, the pronounced heterogeneity in segmental dynamics around T_g^{PEA} as estimated by the wide dispersions of motional activation energies, 'plurality of glass transitions' and discrete manifestation of a few separate types of segmental relaxations in the CR spectra, were observed. All the effects were totally understandable in framework of decreasing the motional cooperativity and different constraining of PEA dynamics by a rigid PIA phase. As a result, for the membranes with high PEA content, e.g. 60 or 80%, the coefficients for organic vapors were 2 or 3 orders of magnitude higher than those of air gases [7]. It should be noted in conclusion that the results of dielectric relaxation measurements, performed for the same hybrid networks and presented in the part II of this article [26], are also in a total accordance with the data discussed. These clearly suggest appearance of long-range connectivity of the PEA component, providing increased diffusion ability for organic vapors, starting from PEA content of about 70 wt% in the hybrids.

Acknowledgements

The authors are grateful to the Russian Fund for Basic Research (RFBR grant 00-03-33173), INTAS (project 97-1936), and NATO (PST.EV.97310 grant for V.A.B.) for financial support of this research.

References

[1] Kimmerle K, Bell CM, Gudernatsch W. J Membr Sci 1988;36:477.
[2] Baker RW, Yioshioka N, Mohr JM, Khan AJ. J Membr Sci 1987;31:259.
[3] Matsumoto K, Ishii K, Kuroda T, Inoue K, Iwama A. Polym J 1991;23:491.
[4] Sysel P, Sindelar V, Fries K, Hynek V, Sipek M. Proceedings of the Fifth European Technical Symposium on Polyimides and High Performance Functional Polymers, Montpellier; 1999. PVI. 2, ISIM.
[5] Feng X, Sourirajan S, Tezel H, Matsuura T. J Appl Polym Sci 1991;43:1071.
[6] Deng S, Tremblay A, Matsuura T. J Appl Polym Sci 1998;69:371.
[7] Sindelar V, Sysel P, Hynek V, Friess K, Sipek M, Castaneda N. Collect Czech Chem Commun 2001;66:533.
[8] Zuo M, Takeichi T. J Polym Sci, Part A: Polym Chem 1997;35:3745.
[9] Zuo M, Xiang Q, Takeichi T. Polymer 1998;39:6883.
[10] Moynihan CT, Eastel AJ, Wilder J. J Phys Chem 1974;78:2673.
[11] Bershtein VA, Egorov VM. Differential scanning calorimetry of polymers. Physics, chemistry, analysis, technology. New York: Ellis Horwood; 1994.
[12] Peschanskaya NN, Yakushev PN, Sinani AB, Bershtein VA. Thermochim Acta 1994;238:429.
[13] Peschanskaya NN, Yakushev PN, Sinani AB, Bershtein VA. Macromol Symp 1997;119:79.
[14] Bershtein VA, Yakushev PN, Karabanova L, Sergeeva L, Pissis P. J Polym Sci, Part B: Polym Phys 1999;37:429.

[15] Bershtein VA, Yakushev PN, Peschanskaya NN. Macromol Symp 1999;147:73.
[16] Bershtein VA, Peschanskaya NN, Halary JL, Monnerie L. Polymer 1999;40:6687.
[17] Bershtein VA, Egorova LM, Egorov VM, Peschanskaya NN, Yakushev PN, Keating MY, Flexman EA, Kassal RJ, Schodt KP. J Macromol Sci, Phys 2002;41:797.
[18] Beacage C, Schaefer DW. J Non-Cryst Solids 1994;173:797.
[19] Glatter O, Kratky O. Small angle X-ray scattering. London: Academic Press; 1982.
[20] Wunderlich B. Macromolecular physics. Crystal melting, vol. 3. New York: Academic Press; 1980.
[21] Bershtein VA, Egorova LM, Prud'homme RE. J Macromol Sci, Phys 1997;36:513.
[22] Bershtein VA, Egorova LM, Sysel P. J Macromol Sci, Phys 1998;37:747.
[23] Bershtein VA, Egorov VM, Egorova LM, Sysel P, Zgonnik VN. J Non-Cryst Solids 1998;235–237:476.
[24] Bershtein VA, Egorov VM, Egorova LM, Yakushev PN, Fainleib AM, Pissis P, Sysel P. NATAS 2000 Proceedings, 604, Orlando.
[25] Bershtein VA, Egorova LM, Ryzhov VA, Yakushev PN, Fainleib AM, Shantalii TA, Pissis P. J Macromol Sci, Phys 2001;40:109.
[26] Kanapitsas A, Pissis P, Delides CG, Sysel P, Sindelar V, Bershtein VA. Polymer 2002; in press.